

Observation of an Inverse Turbulent-Wave Cascade in a Driven Quantum Gas

Andrey Karailiev,¹ Martin Gazo,¹ Maciej Gałka,^{1,2} Christoph Eigen,¹ Tanish Satoor,¹ and Zoran Hadzibabic¹

¹*Cavendish Laboratory, University of Cambridge, J. J. Thomson Avenue, Cambridge CB3 0HE, United Kingdom*

²*Physikalisches Institut der Universität Heidelberg, Im Neuenheimer Feld 226, 69120 Heidelberg, Germany*

We observe an inverse turbulent-wave cascade, from small to large lengthscales, in a driven homogeneous 2D Bose gas. Starting with an equilibrium condensate, we drive the gas isotropically on a lengthscale much smaller than its size, and observe a nonthermal population of modes with wavelengths larger than the drive one. At long drive times, the gas exhibits a steady nonthermal momentum distribution. At lengthscales increasing from the drive one to the system size, this distribution features in turn: (i) a power-law spectrum with an exponent close to the analytical result for a particle cascade in weak-wave turbulence, and (ii) a spectrum reminiscent of a nonthermal fixed point associated with universal coarsening in an isolated 2D gas. In further experiments, based on anisotropic driving, we reveal the complete qualitative picture of how the steady-state cascade forms.

Richardson's direct cascade [1–3], which transports excitations from large to small lengthscales, provides a canonical picture of turbulence and underpins its modern understanding in systems ranging from interplanetary plasmas to financial markets [4, 5]. However, depending on the transport-conserved quantities, turbulence can also feature inverse cascades [6], from small to large lengthscales (see Fig. 1). Such inverse cascades, like the direct ones, are naturally revealed in momentum space, and their key predicted signatures are nonthermal, power-law spectra of quantities such as energy or wave amplitude. For vortex-dominated turbulence, inverse cascades are seen [7–12], for example, in Jupiter's atmosphere [9] and Onsager's vortex clustering [10–12]. For wave turbulence, they have been predicted for systems including gravitational waves in the early Universe [13, 14] and magnetized plasmas in neutron stars [15, 16]. Experimentally, evidence for a decaying inverse wave cascade was observed in nonlinear optics [17–19], while evidence of a steady-state one was observed for surface waves on fluids, using spatially local measurements in the time domain [20–22], but it has remained an outstanding goal to observe a steady-state inverse wave cascade directly in momentum space.

Ultracold Bose gases present an ideal system for studies of wave turbulence on all relevant lengthscales and with well controlled driving and dissipation, as was previously demonstrated for a direct cascade in both three [23–25] and two dimensions [26]. In this Letter we realize and study an inverse turbulent-wave cascade in a homogeneous 2D Bose gas [27, 28], by continuously driving it on a lengthscale much smaller than its size. Starting with an equilibrium condensate and isotropically exciting particles to a large wavenumber k_F , at long times we observe a stationary nonthermal momentum distribution n_k . For wavenumbers $k_\xi \lesssim k \lesssim k_F$, where $1/k_\xi$ is the healing length of the initial condensate, we observe a power-law spectrum $n_k \propto k^{-\gamma}$, with the exponent $\gamma = 1.55(15)$ close to the analytical result $\gamma = 4/3$ for a particle cascade in weak-wave turbulence (WWT) in a 2D Bose gas [29]. At lower k this behavior breaks down, but n_k also differs from that of the equilibrium condensate. Instead, it shows similarity to the spectrum associated with a nonthermal fixed point (NTFP) [30] that characterizes coarsening in an isolated 2D Bose gas [31, 32]; this is consistent with the system effec-

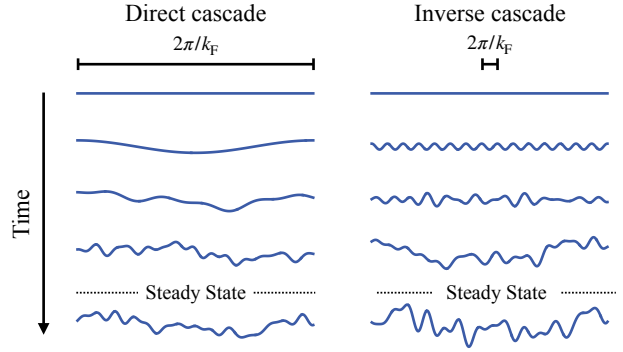


FIG. 1. Real-space cartoons of direct and inverse cascades. The direct cascade corresponds to the transport of excitations from large to small lengthscales (small to large wavenumbers), and the inverse one to transport from small to large lengthscales. Here, starting at time $t = 0$, the system is continuously driven at the wavenumber k_F ; on the left $1/k_F$ is large and oscillations on ever-smaller lengthscales appear as the system evolves, while on the right $1/k_F$ is small and larger-scale oscillations appear. For weak-wave turbulence in a Bose gas, the direct cascade with an idealized sink (dissipation) at $k_D \rightarrow \infty$ corresponds to a scale-invariant energy flux in momentum space, without any particle flux. Similarly, the inverse cascade with a sink at $k_D \rightarrow 0$ corresponds to a pure particle flux, without any energy flux. In both cases, the quantitative signature of a steady-state cascade (established in finite time for a finite k_D) is a nonthermal power-law distribution of mode occupations.

tively behaving as strongly interacting at large lengthscales. We also show that the salient features of the cascade survive for anisotropic (uniaxial) driving, and study the dynamics of the steady-state formation, observing qualitative agreement with theory [33–36].

We start with a 2D quasi-pure ^{39}K condensate of 5×10^4 atoms in the lowest hyperfine state, confined in the x - y plane by a circular optical box trap of radius $R = 22 \mu\text{m}$ and depth $U_D = k_B \times 150 \text{ nK}$; the gas is confined to the plane by a harmonic trap with frequency $\omega_z/(2\pi) = 1.5 \text{ kHz}$ [37]. We set the s -wave scattering length a to $30 a_0$ (where a_0 is the Bohr radius) using the 402.7-G Feshbach resonance [38], so the dimensionless interaction parameter is $\tilde{g} = a\sqrt{8\pi m\omega_z/\hbar} = 0.02$ (where m is the atom mass) [39]. The particle density is

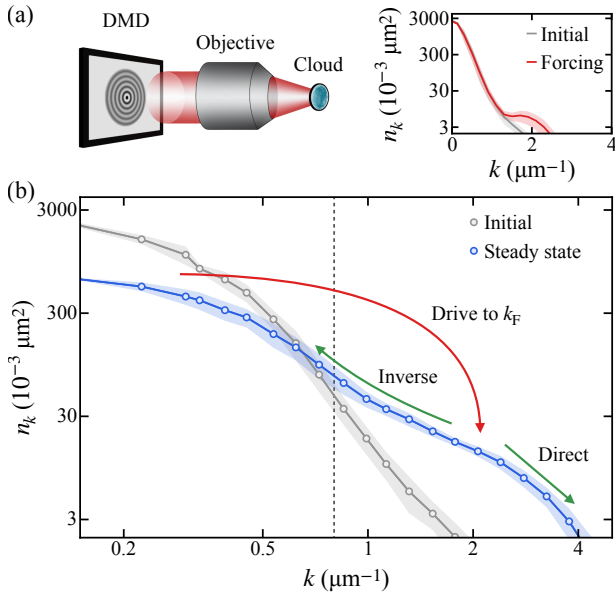


FIG. 2. Forcing and steady state. (a) Left: we drive our box-trapped atomic cloud of radius $R = 22 \mu\text{m}$ isotropically at $k_F \approx 2.1 \mu\text{m}^{-1} \gg 1/R$, using a digital micromirror device (DMD) to create a temporally oscillating potential [46]. Right: momentum distribution after two drive periods (red) shows excitations above the initial equilibrium state (gray). (b) Far-from-equilibrium steady state (blue), shown for $\omega t/(2\pi) = 200$ and contrasted with the initial equilibrium distribution (gray); the dashed line indicates $k_\xi = 0.8 \mu\text{m}^{-1}$. In both panels, the lines and points show azimuthally-averaged data, and the shading indicates azimuthal variations (standard deviation). From hereon (Figs. 3 and 4) we show just the azimuthal averages.

$n = 33 \mu\text{m}^{-2}$, the inverse healing length is $k_\xi = \sqrt{gn} \approx 0.8 \mu\text{m}^{-1}$, and the trap depth sets the high- k dissipation scale, $k_D = \sqrt{2mU_D}/\hbar \approx 5 \mu\text{m}^{-1}$ [24]. We use matter-wave focusing [32, 40] to measure the 2D momentum distributions n_k , which we normalize so that $\int n_k d^2\mathbf{k} = 1$.

As in theoretical studies [29, 41–43], we drive the system isotropically at $|\mathbf{k}| = k_F \gg 1/R$; however, note that theorists typically consider particles injected into an initially empty system, whereas the particles we inject at k_F initially come from the condensate and are at later times recirculated from the low- k states. As illustrated in Fig. 2(a), we use a digital micromirror device (DMD) to project onto the atomic cloud a grayscale [44, 45] radially symmetric driving potential, $U(r, t) = f(r) \sin(\omega t)$, where $f(r)$ is chosen to mimic the spatial structure of the excited mode [46]. The approximate radial period of $f(r)$ is $3.0 \mu\text{m}$, which sets $2\pi/k_F$, so $k_F = 2.1 \mu\text{m}^{-1}$. Our chosen drive frequency, $\omega/(2\pi) = 710 \text{ Hz}$, matches the Bogoliubov-dispersion $\omega(k_F)$ [47].

At long drive times, $\omega t/(2\pi) \geq 75$, we observe a (quasi-)steady far-from-equilibrium n_k , such as shown in Fig. 2(b) for $\omega t/(2\pi) = 200$. As indicated by the arrows, our driving at k_F (red) results in both inverse and direct cascades (green). Since our k_D is not infinite, the direct cascade carries a nonzero particle flux [24] and results in a slow reduction of the total atom number (by 30% between $\omega t/(2\pi) = 75$ and 200), but

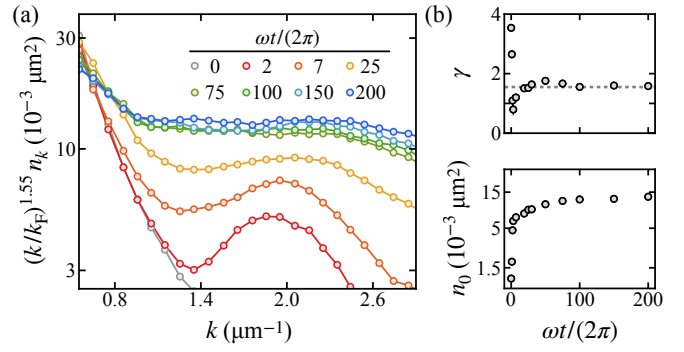


FIG. 3. Steady-state n_k at $k_\xi \lesssim k \lesssim k_F$. (a) The flatness of the compensated spectra, $(k/k_F)^{1.55} n_k$, shows that the nearly stationary long-time distributions are close to the power-law form $n_k = n_0 (k/k_F)^{-\gamma}$, with exponent $\gamma = 1.55$. The analytical result for a particle cascade in WWT is $\gamma = 4/3$. (b) Cascade amplitude, n_0 , and exponent, γ , extracted from power-law fits of n_k for $k = 1.0\text{--}2.1 \mu\text{m}^{-1}$; note that for $\omega t/(2\pi) < 50$ the distribution is not really a power law in this k -range. The dashed line shows $\gamma = 1.55$.

we find that the normalized n_k remains essentially stationary. Here we focus on the inverse cascade, while the direct one was studied with low- k_F driving in [26]; in that case $n_k \propto k^{-2.9}$ was observed [indicated in Fig. 2(b) by the slope of the arrow].

In Fig. 3 we focus on the spectral range $k_\xi \lesssim k \lesssim k_F$, where the equilibrium dispersion relation is particle-like. In Fig. 3(a) we show the evolution of n_k , which at long times is nearly stationary and shows the hallmark feature of a turbulent cascade: a power-law $n_k = n_0 (k/k_F)^{-\gamma}$. Our exponent $\gamma = 1.55(15)$ is close to $4/3$, the analytical result for a particle cascade in WWT theory for weakly interacting 2D Bose gases [29] (see also [48]); the discrepancy between the two could arise due to finite-size effects [25, 26, 31, 43, 49]. In Fig. 3(b) we summarize the system evolution towards the steady state by plotting

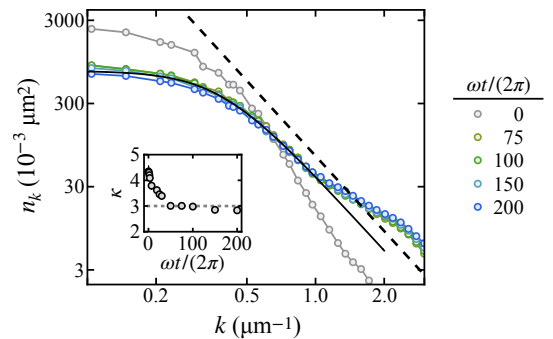


FIG. 4. Steady-state n_k at $k \lesssim k_\xi$. At long times, n_k for $k \leq 1 \mu\text{m}^{-1}$ is captured well by $n_k \propto 1/(1 + (k/k_0)^\kappa)$ with exponent $\kappa = 3$ (solid black line; the dashed line shows the power-law $n_k \propto k^{-3}$). The same form of n_k , with the same κ , characterizes coarsening in an isolated 2D Bose gas, but in that case k_0 decreases algebraically in time, whereas here, under continuous driving, it remains constant ($\approx 0.4 \mu\text{m}^{-1}$). In this spectral range our n_k is at all times captured reasonably well by the same functional form, with κ , fitted as a free parameter, evolving as shown in the inset.

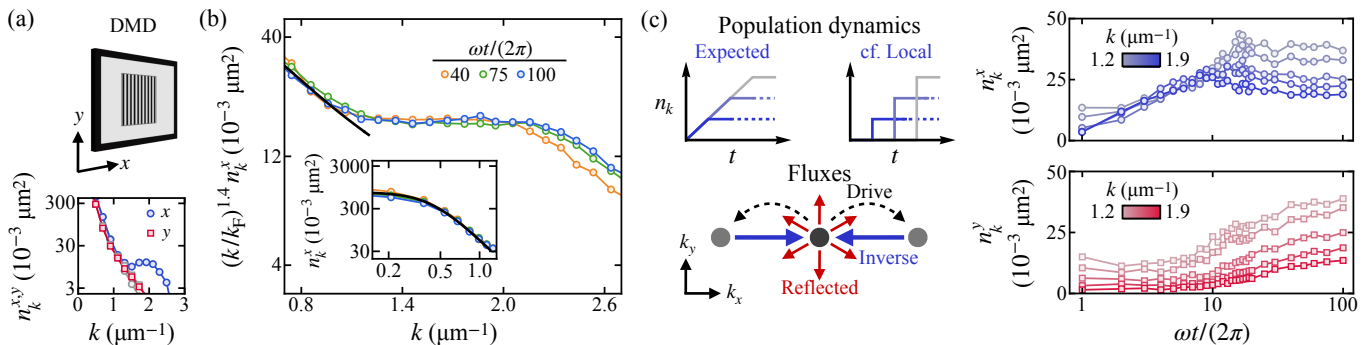


FIG. 5. Steady state and cascade-formation dynamics for anisotropic driving. (a) Here we use a square box trap and change the DMD pattern to drive the gas uniaxially, at $(k_x, k_y) = (\pm k_F, 0)$, with the same k_F as in Figs. 2-4. The bottom panel shows, for $\omega t/(2\pi) = 2$ (in color; cf. $t = 0$ in gray), that excitations are created along x and not along y . Here $n_k^x(k)$ (resp. $n_k^y(k)$) is the average population of modes with wavevectors within $\pi/8$ radians of the x (resp. y) axis. (b) Along x we observe essentially the same steady state as for isotropic driving, with $\gamma = 1.4(1)$ for $k_\xi \lesssim k \lesssim k_F$ and $\kappa = 3$ (black line) at lower k ; the inset shows a zoom-in on low k . (c) Population dynamics along x and y . The top cartoons show the expected non-local dynamics along the drive and, for comparison, what the dynamics would be if they were local; darker blue corresponds to higher k . The bottom cartoon shows the uniaxial drive to $(\pm k_F, 0)$, the inverse particle flux, and the reflected flux; for isotropic driving both fluxes are isotropic, while here we expect the inverse one to be uniaxial and the reflected one to be omnidirectional. Our n_k^x data (top panel) are consistent with the expected non-local dynamics, while the n_k^y data (bottom panel) reveal the delayed reflected flux.

$n_0(t)$ and $\gamma(t)$ obtained from power-law fits of n_k .

At lower k , this behavior breaks down. Here, the initial condensate is replaced by a nonthermal distribution that is at long times captured well by $n_k \propto 1/(1 + (k/k_0)^\kappa)$ with exponent $\kappa = 3$ (see Fig. 4). Interestingly, the same form of n_k , with the same κ , characterizes the particle flow to low k during coarsening in an isolated 2D Bose gas [31, 32], which is understood in terms of the system being attracted to an NTFP [30]. However, during coarsening k_0 decreases algebraically in time, whereas here, under continuous driving, the excitations are recirculated in k -space and k_0 is constant [50]. Tentatively, this can be interpreted as the system being stabilized near an NTFP.

The exponents γ and κ are in fact predicted within the same theoretical framework of the momentum-space wave-kinetic equation, but in the weakly- and strongly-interacting limits, respectively [31, 51]. Our observations are thus also consistent with the theoretical expectation that the system behaves as weakly interacting on lengthscales smaller than $1/k_\xi$, but as strongly interacting on larger lengthscales.

We now turn to experiments where we change the driving potential to further study the cascade-formation dynamics. Here we drive the gas along only one direction, x [see Fig. 5(a)], and also switch to a square box trap (of side length $30 \mu\text{m}$), while keeping n , k_ξ , and k_F the same as in Figs. 2-4.

First, in Fig. 5(a) we show, for $\omega t/(2\pi) = 2$, that the injection of excitations into modes with wavevectors close to the x axis is similar to before [see Fig. 2(a)], but the modes with wavevectors close to the y axis are not directly excited by the drive. Here $n_k^x(k)$ denotes populations averaged over \mathbf{k} vectors within $\pi/8$ radians of the x axis (parallel to the drive), and $n_k^y(k)$ denotes populations of modes with wavevectors within $\pi/8$ radians of the y axis (perpendicular to the drive).

Next, in Fig. 5(b) we show that along the drive direction the long-time behavior is essentially the same as for the isotropic

drive, which implies that the cascade dynamics are azimuthally local: for $k_\xi \lesssim k \lesssim k_F$ we observe a stationary power-law n_k^x , with $\gamma = 1.4(1)$, while n_k^x at lower k is captured well by the same form as in Fig. 4, with $\kappa = 3$. Note that here the steady state is reached for $\omega t/(2\pi) \approx 40$.

Finally, in Fig. 5(c) we study the cascade formation by looking at the dynamics of both n_k^x and n_k^y ; the cartoons outline the two key theoretical concepts that our data support. First, for isotropic driving, n_k at different k are expected to initially grow in unison [33, 35], which means that the inverse cascade, in contrast to the direct one [26], is not local in k -space (see top cartoons). Here, this expectation should apply (only) to the dynamics of n_k^x , parallel to the drive, and indeed matches our observations. Second, in theory, the inverse particle flux also results in a delayed counter-propagating ‘reflected’ flux [34, 36], which is formally required for the steady state to be established [52]. We do not observe this flux directly for isotropic driving, but here it is revealed perpendicular to the drive, where there is no inverse flux (see bottom cartoon): the n_k^y populations do grow, but only with a delay, after the growth of n_k^x (for $k \gtrsim k_\xi$) is nearly complete. At long times, n_k^y is also close to a power-law, approximately $\propto k^{-2.4}$ (not shown, see [46]), but we are not aware of any prediction for this purely reflected cascade.

In conclusion, by measuring directly in k -space and on all relevant lengthscales and timescales, we observe both the statistical properties of a steady-state inverse turbulent-wave cascade in a driven 2D Bose gas, and the key qualitative features of its formation dynamics. In the future, it would be interesting to measure the underlying cascade fluxes [24] and test the expected self-similar evolution at pre-steady-state times [35, 36]. Such studies would greatly benefit from an extension of the cascade spectral range (here limited by our optical resolution [46]), which could be increased by an order of magnitude using an

optical lattice to drive the gas, capitalizing on our observation that uniaxial driving preserves the key features of the cascade. At low k , the stationary nonthermal spectrum we observe has a characteristic lengthscale ($1/k_0$), whose origin could be linked to the recently proposed concept of emergent lengthscales in nonlinear driven systems [53].

The supporting data for this Letter are available in the Apollo repository [54].

We thank Panagiotis Christodoulou and Nishant Dogra for early contributions and Gevorg Martirosyan, Jiří Etrych, Nir Navon, Jürgen Berges, and Aleksas Mazeliauskas for discussions and comments on the manuscript. This work was supported by EPSRC [Grant No. EP/P009565/1], ERC (UniFlat), and STFC [Grant No. ST/T006056/1]. M. Gałka acknowledges support from Germany's Excellence Strategy EXC2181/1-390900948 (Heidelberg Excellence Cluster STRUCTURES). Z.H. acknowledges support from the Royal Society Wolfson Fellowship.

-
- [1] L. F. Richardson, *Weather prediction by numerical process* (Cambridge University Press, 1922).
- [2] A. N. Kolmogorov, The local structure of turbulence in incompressible viscous fluid for very large Reynolds numbers, *Dokl. Akad. Nauk SSSR* **30**, 299 (1941).
- [3] A. Obukhov, On the distribution of energy in the spectrum of turbulent flow, *Dokl. Akad. Nauk SSSR* **32**, 22 (1941).
- [4] L. Sorriso-Valvo, R. Marino, V. Carbone, A. Noullez, F. Lepreti, P. Veltri, R. Bruno, B. Bavassano, and E. Pietropaolo, Observation of Inertial Energy Cascade in Interplanetary Space Plasma, *Phys. Rev. Lett.* **99**, 115001 (2007).
- [5] S. Ghashghaie, W. Breymann, J. Peinke, P. Talkner, and Y. Dodge, Turbulent cascades in foreign exchange markets, *Nature* **381**, 767 (1996).
- [6] R. H. Kraichnan, Inertial Ranges in Two-dimensional Turbulence, *Phys. Fluids* **10**, 1417 (1967).
- [7] J. Paret and P. Tabeling, Experimental Observation of the Two-Dimensional Inverse Energy Cascade, *Phys. Rev. Lett.* **79**, 4162 (1997).
- [8] M. A. Rutgers, Forced 2D Turbulence: Experimental Evidence of Simultaneous Inverse Energy and Forward Enstrophy Cascades, *Phys. Rev. Lett.* **81**, 2244 (1998).
- [9] R. M. B. Young and P. L. Read, Forward and inverse kinetic energy cascades in Jupiter's turbulent weather layer, *Nat. Phys.* **13**, 1135 (2017).
- [10] G. Gauthier, M. T. Reeves, X. Yu, A. S. Bradley, M. A. Baker, T. A. Bell, H. Rubinsztein-Dunlop, M. J. Davis, and T. W. Neely, Giant vortex clusters in a two-dimensional quantum fluid, *Science* **364**, 1264 (2019).
- [11] S. P. Johnstone, A. J. Groszek, P. T. Starkey, C. J. Billington, T. P. Simula, and K. Helmerston, Evolution of large-scale flow from turbulence in a two-dimensional superfluid, *Science* **364**, 1267 (2019).
- [12] R. Panico, P. Comaron, M. Matuszewski, A. S. Lanotte, D. Trypogeorgos, G. Gigli, M. D. Giorgi, V. Ardizzone, D. Sanvitto, and D. Ballarini, Onset of vortex clustering and inverse energy cascade in dissipative quantum fluids, *Nat. Photon.* **17**, 451 (2023).
- [13] S. Galtier and S. V. Nazarenko, Turbulence of Weak Gravitational Waves in the Early Universe, *Phys. Rev. Lett.* **119**, 221101 (2017).
- [14] S. Galtier, S. V. Nazarenko, Éric Buchlin, and S. Thalabard, Nonlinear diffusion models for gravitational wave turbulence, *Phys. D: Nonlinear Phenom.* **390**, 84 (2019).
- [15] D. Biskamp, E. Schwarz, and J. F. Drake, Two-Dimensional Electron Magnetohydrodynamic Turbulence, *Phys. Rev. Lett.* **76**, 1264 (1996).
- [16] A. Brandenburg, Hall cascade with fractional magnetic helicity in neutron star crusts, *Astrophys. J.* **901**, 18 (2020).
- [17] U. Bortolozzo, J. Laurie, S. Nazarenko, and S. Residori, Optical wave turbulence and the condensation of light, *J. Opt. Soc. Am. B* **26**, 2280 (2009).
- [18] J. Laurie, U. Bortolozzo, S. Nazarenko, and S. Residori, One-dimensional optical wave turbulence: Experiment and theory, *Phys. Rep.* **514**, 121 (2012).
- [19] D. Pierangeli, F. Di Mei, G. Di Domenico, A. J. Agranat, C. Conti, and E. DelRe, Turbulent Transitions in Optical Wave Propagation, *Phys. Rev. Lett.* **117**, 183902 (2016).
- [20] L. Deike, C. Laroche, and E. Falcon, Experimental study of the inverse cascade in gravity wave turbulence, *Europhys. Lett.* **96**, 34004 (2011).
- [21] E. Falcon, G. Michel, G. Prabhudesai, A. Cazaubiel, M. Berhanu, N. Mordant, S. Aumaître, and F. Bonnefoy, Saturation of the Inverse Cascade in Surface Gravity-Wave Turbulence, *Phys. Rev. Lett.* **125**, 134501 (2020).
- [22] E. Falcon and N. Mordant, Experiments in surface gravity-capillary wave turbulence, *Annu. Rev. Fluid Mech.* **54**, 1–25 (2022).
- [23] N. Navon, A. L. Gaunt, R. P. Smith, and Z. Hadzibabic, Emergence of a turbulent cascade in a quantum gas, *Nature* **539**, 72 (2016).
- [24] N. Navon, C. Eigen, J. Zhang, R. Lopes, A. L. Gaunt, K. Fujimoto, M. Tsubota, R. P. Smith, and Z. Hadzibabic, Synthetic dissipation and cascade fluxes in a turbulent quantum gas, *Science* **366**, 382 (2019).
- [25] L. H. Dogra, G. Martirosyan, T. A. Hilker, J. A. P. Glidden, J. Etrych, A. Cao, C. Eigen, R. P. Smith, and Z. Hadzibabic, Universal equation of state for wave turbulence in a quantum gas, *Nature* **620**, 521 (2023).
- [26] M. Gałka, P. Christodoulou, M. Gazo, A. Karailiev, N. Dogra, J. Schmitt, and Z. Hadzibabic, Emergence of Isotropy and Dynamic Scaling in 2D Wave Turbulence in a Homogeneous Bose Gas, *Phys. Rev. Lett.* **129**, 190402 (2022).
- [27] L. Chomaz, L. Corman, T. Bienaimé, R. Desbuquois, C. Weitenberg, S. Nascimbène, J. Beugnon, and J. Dalibard, Emergence of coherence via transverse condensation in a uniform quasi-two-dimensional Bose gas, *Nat. Commun.* **6**, 6162 (2015).
- [28] N. Navon, R. P. Smith, and Z. Hadzibabic, Quantum gases in optical boxes, *Nat. Phys.* **17**, 1334 (2021).
- [29] S. Dyachenko, A. C. Newell, A. Pushkarev, and V. E. Zakharov, Optical turbulence: weak turbulence, condensates and collapsing filaments in the nonlinear Schrödinger equation, *Phys. D: Nonlinear Phenom.* **57**, 96 (1992).
- [30] J. Berges, A. Rothkopf, and J. Schmidt, Nonthermal Fixed Points: Effective Weak Coupling for Strongly Correlated Systems Far from Equilibrium, *Phys. Rev. Lett.* **101**, 041603 (2008).
- [31] I. Chantesana, A. Piñeiro Orioli, and T. Gasenzer, Kinetic theory of nonthermal fixed points in a Bose gas, *Phys. Rev. A* **99**, 043620 (2019).
- [32] M. Gazo, A. Karailiev, T. Satoor, C. Eigen, M. Gałka, and Z. Hadzibabic, Universal Coarsening in a Homogeneous Two-Dimensional Bose Gas, [arXiv:2312.09248](https://arxiv.org/abs/2312.09248) (2023).
- [33] D. V. Semikoz and I. I. Tkachev, Kinetics of Bose Condensation,

- Phys. Rev. Lett. **74**, 3093 (1995).
- [34] S. Galtier, S. V. Nazarenko, A. C. Newell, and A. Pouquet, A weak turbulence theory for incompressible magnetohydrodynamics, *J. Plasma Phys.* **63**, 447 (2000).
- [35] B. Semisalov, V. Grebenev, S. Medvedev, and S. Nazarenko, Numerical analysis of a self-similar turbulent flow in Bose–Einstein condensates, *Commun. Nonlinear Sci. Numer. Simul.* **102**, 105903 (2021).
- [36] Y. Zhu, B. Semisalov, G. Krstulovic, and S. Nazarenko, Self-similar evolution of wave turbulence in Gross-Pitaevskii system, *Phys. Rev. E* **108**, 064207 (2023).
- [37] P. Christodoulou, M. Gałka, N. Dogra, R. Lopes, J. Schmitt, and Z. Hadzibabic, Observation of first and second sound in a BKT superfluid, *Nature* **594**, 191 (2021).
- [38] J. Etrych, G. Martirosyan, A. Cao, J. A. P. Glidden, L. H. Dogra, J. M. Hutson, Z. Hadzibabic, and C. Eigen, Pinpointing Feshbach resonances and testing Efimov universalities in ^{39}K , *Phys. Rev. Res.* **5**, 013174 (2023).
- [39] Z. Hadzibabic and J. Dalibard, Two-dimensional Bose fluids: An atomic physics perspective, *Riv. del Nuovo Cim.* **34**, 389 (2011).
- [40] S. Tung, G. Lamporesi, D. Lobser, L. Xia, and E. A. Cornell, Observation of the Presuperfluid Regime in a Two-Dimensional Bose Gas, *Phys. Rev. Lett.* **105**, 230408 (2010).
- [41] S. Nazarenko and M. Onorato, Wave turbulence and vortices in Bose-Einstein condensation, *Phys. D: Nonlinear Phenom.* **219**, 1 (2006).
- [42] S. Nazarenko, *Wave Turbulence* (Springer, 2011).
- [43] Y. Zhu, B. Semisalov, G. Krstulovic, and S. Nazarenko, Direct and Inverse Cascades in Turbulent Bose-Einstein Condensates, *Phys. Rev. Lett.* **130**, 133001 (2023).
- [44] G. Gauthier, I. Lenton, N. M. Parry, M. Baker, M. J. Davis, H. Rubinsztein-Dunlop, and T. W. Neely, Direct imaging of a digital-micromirror device for configurable microscopic optical potentials, *Optica* **3**, 1136 (2016).
- [45] Y.-Q. Zou, E. L. Cerf, B. Bakkali-Hassani, C. Maury, G. Chauveau, P. C. M. Castilho, R. Saint-Jalm, S. Nascimbene, J. Dalibard, and J. Beugnon, Optical control of the density and spin spatial profiles of a planar Bose gas, *J. Phys. B: At. Mol. Opt. Phys.* **54**, 08LT01 (2021).
- [46] See Supplemental Material for details of the DMD driving and an additional panel for Fig. 5.
- [47] For our strong drive, we observe efficient excitation up to about 120 Hz away from 710 Hz.
- [48] We note that the validity of the result $\gamma = 4/3$ was questioned by the authors themselves [29], because it is formally not self-consistent. In 1D optical-wave turbulence the same type of result is also formally not self-consistent, but does agree quite well with the experiments [18].
- [49] G. Martirosyan, K. Fujimoto, and N. Navon, An Equation of State for Turbulence in the Gross-Pitaevskii Model, [arXiv:2407.08738](https://arxiv.org/abs/2407.08738) (2024).
- [50] The particle recirculation would be perfect for $k_D/k_F \rightarrow \infty$, such that the direct cascade would not carry away any particles. In our case, the normalized n_k is stationary.
- [51] This is a classical-field Gross–Pitaevskii model, which should be applicable when the mode occupations are much larger than unity. In our case, in steady state, the mode occupations $4\pi^2 n n_k$ range from about 10 at k_F to about 500 for $k \rightarrow 0$.
- [52] The reflected flux is necessary because the inverse cascade has a finite particle capacity; in contrast, the direct cascade has an infinite energy capacity [42].
- [53] X. M. de Wit, M. Fruchart, T. Khain, F. Toschi, and V. Vitelli, Pattern formation by turbulent cascades, *Nature* **627**, 515 (2024).

- [54] A. Karailiev, M. Gazo, M. Gałka, C. Eigen, T. Satoor, and Z. Hadzibabic, Research data supporting “Observation of an Inverse Turbulent-Wave Cascade in a Driven Quantum Gas”, Apollo - University of Cambridge Repository [10.17863/CAM.113609](https://doi.org/10.17863/CAM.113609) (2024).

SUPPLEMENTAL MATERIAL

DMD driving

We use grayscaleing on a digital micromirror device (DMD) to create our time-varying drive potentials. Our imaging resolution is approximately $1.5\ \mu\text{m}$, whereas a DMD pixel corresponds to $0.22\ \mu\text{m}$ in the atomic plane, which gives $(1.5/0.22)^2 \approx 46$ grayscale levels [44, 45]. As in [45], we use an error diffusion algorithm to convert continuous functions into binary masks. The largest k_F we can achieve, of about $2\ \mu\text{m}^{-1}$, is also set by our imaging resolution.

In the circular trap (with radius $R = 22\ \mu\text{m}$) used for Figs. 2-4, radially symmetric excitation modes have the form $J_0(q_n r/R)$, where J_0 is the zeroth-order Bessel function of the first kind and q_n its n^{th} extremum. In the square trap (with side length $L = 30\ \mu\text{m}$) used for Fig. 5, we excite a mode of the form $\cos(n\pi(x + L/2)/L)$.

For the radial and axial driving, respectively, we choose $n = 14$ and 21, which in both cases corresponds to $k_F \approx 2.1\ \mu\text{m}^{-1}$. Note, however, that due to strong driving and imperfect mode-matching some neighboring modes could also be directly excited by the drive; in both cases the closest modes allowed by the symmetry of the drive have k values that differ from our nominal k_F by about $\pm 0.2\ \mu\text{m}^{-1}$.

Additional panel for Fig. 5

The uniaxial driving protocol used for Fig. 5 results in anisotropic momentum distributions at long drive times. In Fig. S1 we show n_k^y for the same times as in Fig. 5(b). The black line corresponds to $n_k^y \propto k^{-2.4}$.

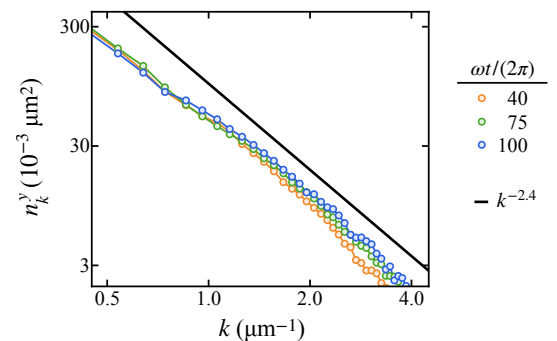


FIG. S1. Long-time momentum distributions n_k^y , perpendicular to the uniaxial drive. The black line corresponds to $n_k^y \propto k^{-2.4}$.